Sunflower Stalk Based Activated Carbon for Supercapacitors

Süperkapasitörler için Ayçiçeği Sapı Temelli Aktif Karbon

Alp Yürüm[ORCID]

Sabanci Sabanci University Nanotechnology Research and Application Center (SUNUM), Sabanci University, İstanbul, Turkey

ABSTRACT

In this study, a combination of physical and chemical activation was used to produce activated carbon from sunflower stalks. The NaOH activated carbon possess a high specific surface area of 2658 m^2/g. The micropore fraction and surface area obtained is much higher than a commercial activated carbon. The electrodes from the activated carbons were electrochemically analyzed in a two-electrode supercapacitor cell with 1 M H_2SO_4 electrolyte. The results show that the high surface area of sunflower activated carbon resulted in significantly high specific capacitance of 207 F/g at 0.05 A/g current density. Moreover, a high energy density of 18.4 Wh/kg was obtained at the power density of 80 W/kg. The results also showed the importance of pore structure on the supercapacitor performance.

Key Words
Sunflower stalk, activated carbon, supercapacitor.

ÖZ

Bu çalışmada, ayçiçeği saplarından aktif karbon üretmek için fiziksel ve kimyasal aktivasyon yöntemlerinin bir bileşimi kullanıldı. NaOH ile aktive edilen aktif karbon, 2658 m^2/g gibi yüksek bir yüzey alanına sahiptir. Elde edilen mikrogözenek oranı ve yüzey alanı mktarı ticari aktif karbonlardan çok daha yüksektir. Aktif karbonlardan elde edilen elektrotlar, ikili süper kapasitör hücresinde, 1 M H_2SO_4 elektrolit ile elektrokimyasal olarak analiz edilmiştir. Sonuçlar, ayçiçeğinden elde edilen yüksek yüzey alanı sayesinde, 0.05 A/g akım yoğunluğunda, önemli derecede yüksek bir kapasitans olan 207 F/g elde edildiğini göstermiştir. Buna ek olarak, 80 W/kg güç yoğunluğunda yüksek bir enerji yoğunluğu değeri olan 18.4 Wh/kg elde edilmiştir. Sonuçlar ayrıca gözenek yapısının süper kapasitör performansı için ne kadar önemli olduğunu da göstermiştir.

Anahtar Kelimeler
Ayçiçeği sapı, aktif karbon, süperkapasitör.

INTRODUCTION

In recent years, due to environmental concerns and energy issues, to recycle agricultural residues has increasing recognition. One interesting application is to use lignocellulosic wastes for the production of activated carbons (ACs) [1-3]. These high surface area materials from carbonaceous sources can be either synthesized with oxidizing gases (steam, air, etc.) or chemicals (H_2SO_4, KOH, etc.) at high temperatures. While the main source is coal, other carbonaceous materials like wood, fruit stones, etc. are also utilized [1, 2]. Activated carbons have a series of micro and mesopores connected to each other. This results in a very high porosity and specific surface area carbon material. The surface area and the pore structure highly depend on the raw material and activation agent used [4-6].

In industry, their high porosity makes them a perfect material as an adsorbent in purification applications. They are also very suitable materials as supports in catalytic reactions. Lately, activated carbons became an attractive material of electric double-layer capacitors (EDCLs) [7, 8]. These devices are a new type of electrical energy storage systems and have high power capabilities with long cycle life. In EDCL, energy is stored by the interaction of surface charges on the electrode and the ion conducting electrolyte. Introduction of low-cost and high specific surface area carbon materials is the main priority for the mass production of these devices. For that reason, lignocellulosic waste-based ACs is an important scientific research area [9-12].

In Thracia region of Turkey, there is a high amount of sunflower oil production but the stalks are industrially useless and they are used only for burning by the local farmers. From an industrial point of view, this a huge waste, considering the potential of these materials. Previous studies have shown that sunflower stalks are an attractive source of material for activated carbon production [13]. These activated carbons have been successfully used for the removal of dyes and heavy metal ions from aqueous solutions.

In this study, sunflower stalks from a local farm were chosen as the cheap lignocellulosic waste. The activation was a combination of chemical and physical processes. Structural characteristics of the synthesized activated carbon were analyzed by different tests. Nevertheless, the final product was studied as a supercapacitor material in an acidic electrolyte. The comparisons with a commercial activated carbon shows the potential of sunflower stalk-based activated carbons as electrode materials in supercapacitors.

MATERIALS and METHODS

Materials

The sunflower stalk used for the activation was obtained from a farm in Kırklareli, a city from the Thracian region of Tukey. For the chemical activation of the carbon source, sodium hydroxide (NaOH) (Sigma-Aldrich, purity 98-100%) was used. Hydrochloric acid (HCl) (Sigma-Aldrich, 37%) was used to wash the samples and sulfuric acid (H_2SO_4) (Sigma-Aldrich, 98%) was used as the electrolyte. For comparison, a commercial coal-based activated carbon (AC) sample (Com) was utilized (Merck).

Synthesis of the activated carbon

For the synthesis of activated carbon, a thermochemical method was followed. This synthesis consists of two steps. At first step, the sunflower pith was dried, peeled and the inner foam-like core was ground. The ground particles (1 mm particles) were carbonized under N2 atmosphere at 500°C (10°C/min heating rate) for 60 minutes. In the second step, the carbonized material was mixed with NaOH with a 3:1 mass ratio (NaOH:char) and distilled (DI) water. After the slurry was stirred for 2 hours, it was dried at 130°C for 4 hours. As the last step, the dried mixture was activated at 700°C (10°C/min) for 120 minutes under an N2 atmosphere. The activated mixture was first washed with 0.1 M HCl and then hot DI water until a neutral pH was reached. After drying (110°C, 24 h), the NaOH activated carbon was labeled as Acna.

Characterization

Textural properties of Acna and Com were determined by a Micromeritics 3Flex Surface Characterization device (at 77 K for nitrogen adsorption and desorption isotherms). The specific surface areas of the samples were calculated from the N2 adsorption isotherm (P/P0 range of 0.03-0.1) using the Brunauer–Emmett–Teller (BET) equation. The total pore volume was calculated according to the volume of liquid nitrogen adsorbed at the relative pressure up to P/P0 = 0.99 [14]. Dubinin-Radushkevic equation was used to determine the micropore volume and the average pore diameter was calculated by the DFT method.

Thermogravimetric analyses and ash content of the carbon materials were determined by NETZSCH Simultane-

ous Thermal Analyzer STA 449 C Jupiter (up to 1000°C – a heating rate of 10°C/min). Fourier Transform Infrared (FTIR) spectroscopic analyses of the samples were performed using a Thermo Scientific's Nicolet iS10 FT-IR spectrometer, between the wavenumbers 4000 and 500 cm^{-1}.

Electrochemical Characterization

Two-electrode symmetrical cells were prepared with AC materials in a split cell setup. After the AC materials were ground, they were mixed with carbon black and polyvinylidene fluoride (PVDF) with an 80:10:10 ratio (AC:carbon black:PVDF). N-methyl-2-pyrrolidone (NMP) was added to the mixture to obtain a slurry and stirred overnight. Stainless steel current collectors were coated with these slurries and dried at 110°C in a vacuum oven. The final coating mass was about 0.4 mg/cm^2. The electrodes were screwed tightly in the split cell. A polypropylene membrane was used as the separator and the electrolyte was 0.1 M H$_2$SO$_4$ solution.

The electrochemical performance of the AC supercapacitor cells was characterized using a PARSTAT MC potentiostat system. The potential range for the cyclic voltammetry (CV) measurement was between 0-0.8 V, and the voltage scanning rate was in a range of 1-200 mV/s. The current densities for the galvanostatic charge and discharge measurements were performed between 0.5-2 A/g under the potential window of 0-0.8 V. The electrochemical impedance spectroscopy (EIS) measurements were recorded in a frequency range of 10 mHz^{-1} MHz with a sinusoid alternative voltage of 10 mV.

RESULTS and DISCUSSION

Material Characterization

The yield of the activation process is an important parameter when producing ACs. It is defined as the final weight of the product at the end of the reaction. After the carbonization of the sunflower stalks at 500°C for 60 minutes, the percent yield was calculated as 34%. This value is reasonable for biochars [15, 16]. At the second step, the biochar is activated with NaOH at 700°C for 120 minutes. Here NaOH breaks the C-O-C and C-C bonds of the char [15, 16]. In the end, after all of the washing and drying steps, the final percent yield was calculated as 19%.

The functional groups which were identified from the FTIR spectrum for the sunflower stalk and AC samples are presented in Table 1 & 2 [14, 17]. The FTIR spectra are also shown in Figure 1. In the spectrum for the sunflower's raw sample, the broadband of O-H stretching at the 3300 to 3000 cm^{-1} range shows the presence of oxygen-containing functional groups in the organic structure of the biomass [18]. During the carbonization and activation, most of the functional groups of the precursor were diminished. The FTIR spectra of the ACs show a loss for most of the functionalization in the region from 3500 to 1600 cm^{-1}. Aliphatic CH stretching around 2900 cm^{-1} also diminished due to complete removal of hydrogen-containing aliphatic groups. The aromatic CO stretching bands between 1300 and 1050 cm^{-1} mostly associated with the plant's cellulose structure.

**Table 1.** Functional groups of sunflower stalk determined by the FTIR.

Wavenumber (cm^{-1})	Functional Group
3331	−OH Stretching
2903	Aliphatic CH Stretching Vibration
1598	Aromatic C=C Ring Stretching
1416	Aromatic C=C Ring Stretching
1318	Aliphatic CH3 Deformation
1203	Aromatic CO− Stretching
1022	Aliphatic Ether C−O and Alcohol C−O Stretching
894	Aromatic Ring

Table 2. Functional groups of AC samples determined by the FTIR.

Wavenumber (cm⁻¹)	Functional Group
1694	C=O Stretching
1461	C=O Stretching in Carboxylic Groups
1287	C−O−C Stretching
1095	C−O−C Asymmetric Stretching
861	Aromatic C−H Ring Stretching

These peaks lost their intensity after the carbonization at 500°C. Because of the activation process, chemical bonds were broken, and most of the functional groups were lost and resembled carbonaceous materials in the literature [19]. At the end of the activation process, the peak related to the aliphatic groups located at around 1400 cm⁻¹ disappeared. The main reason can be the de-composition of lignin structure in the char during the activation which was conducted at 700°C [20]. For comparison reasons, a commercial AC sample, Com, also was characterized. It was seen that the functional group in both synthesized Acna in this study and Com show the same pattern in the FTIR spectra.
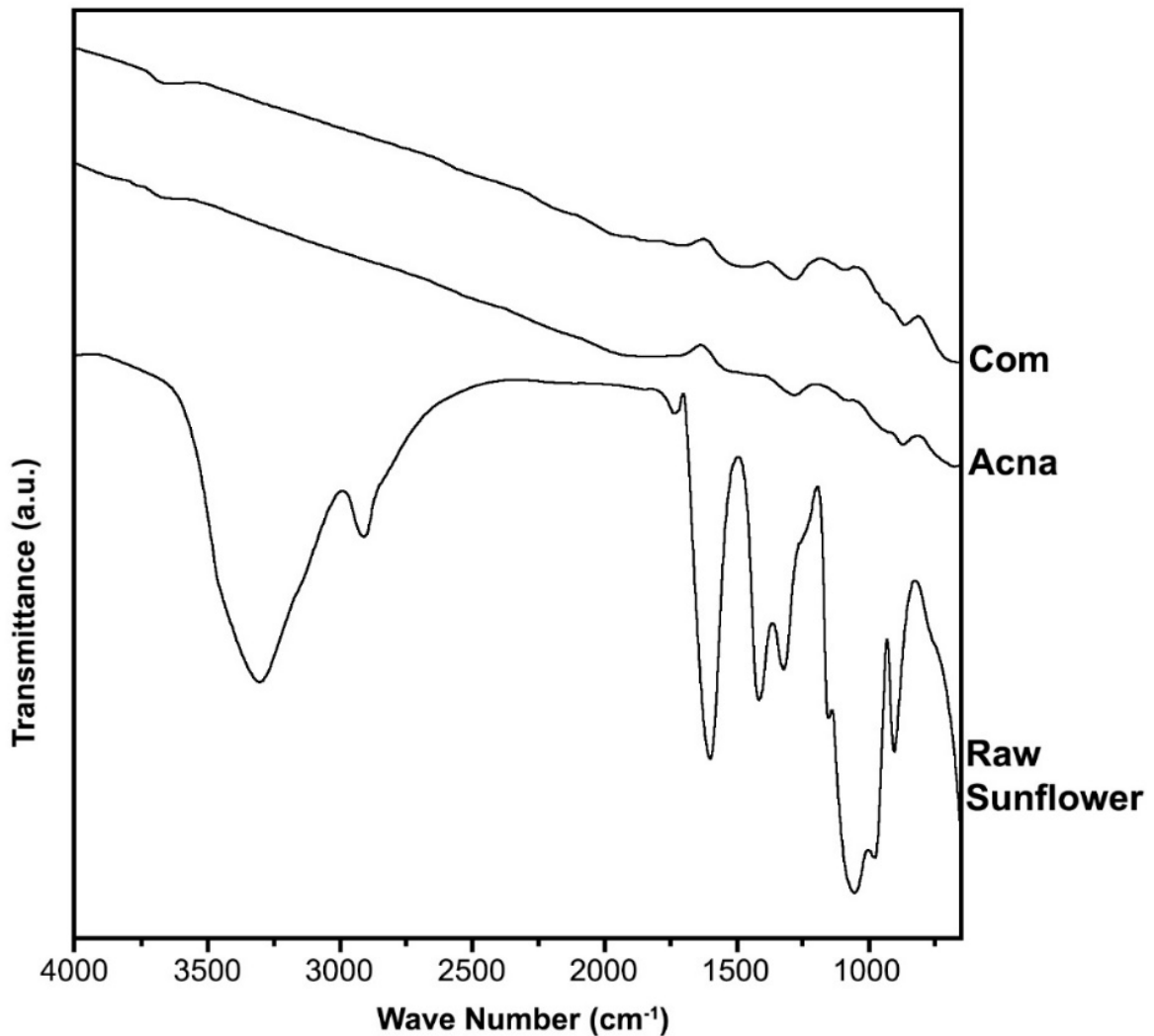
**Figure 1.** FTIR spectra for the sunflower stalk and AC samples.

**Table 3.** Textural properties of the activated carbons.

Sample	SBET (m²/g)	Vtotal (cm³/g)	Vmicro (cm³/g)	Vmeso (cm³/g)	Vmicro/Vtotal (%)	d_{pore} (nm)
Com	754	0.53	0.18	0.35	34	5.8
Acna	2658	1.21	0.88	0.33	69	2.9

Textural Properties

The porous structure of the AC samples was analyzed by obtaining the nitrogen adsorption and desorption isotherms at 77 K. These isotherms are illustrated in Figure 2. Both of the isotherms mainly belong to type I with a very small hysteresis at high P/P0 values (H4). Less steep nitrogen uptake at lower P/P0 means that the materials have a broader pore size distribution, with mainly wide micropores and some mesopores [21]. The type I isotherm, which is also known as Langmuir isotherm, indicated that the adsorbent and adsorbate have high affinity with each other. The textural analysis results of the AC samples are presented in Table 3, where SBET, Vtotal, Vmicro, Vmeso, and dpore are the BET surface area, total pore volume, micropore volume, mesopore volume, and average pore diameter, respectively. These results confirm the isotherm analyses. A wide range of porosity was observed for both Com and Acna, while Acna being more microporous and having higher specific BET surface area.
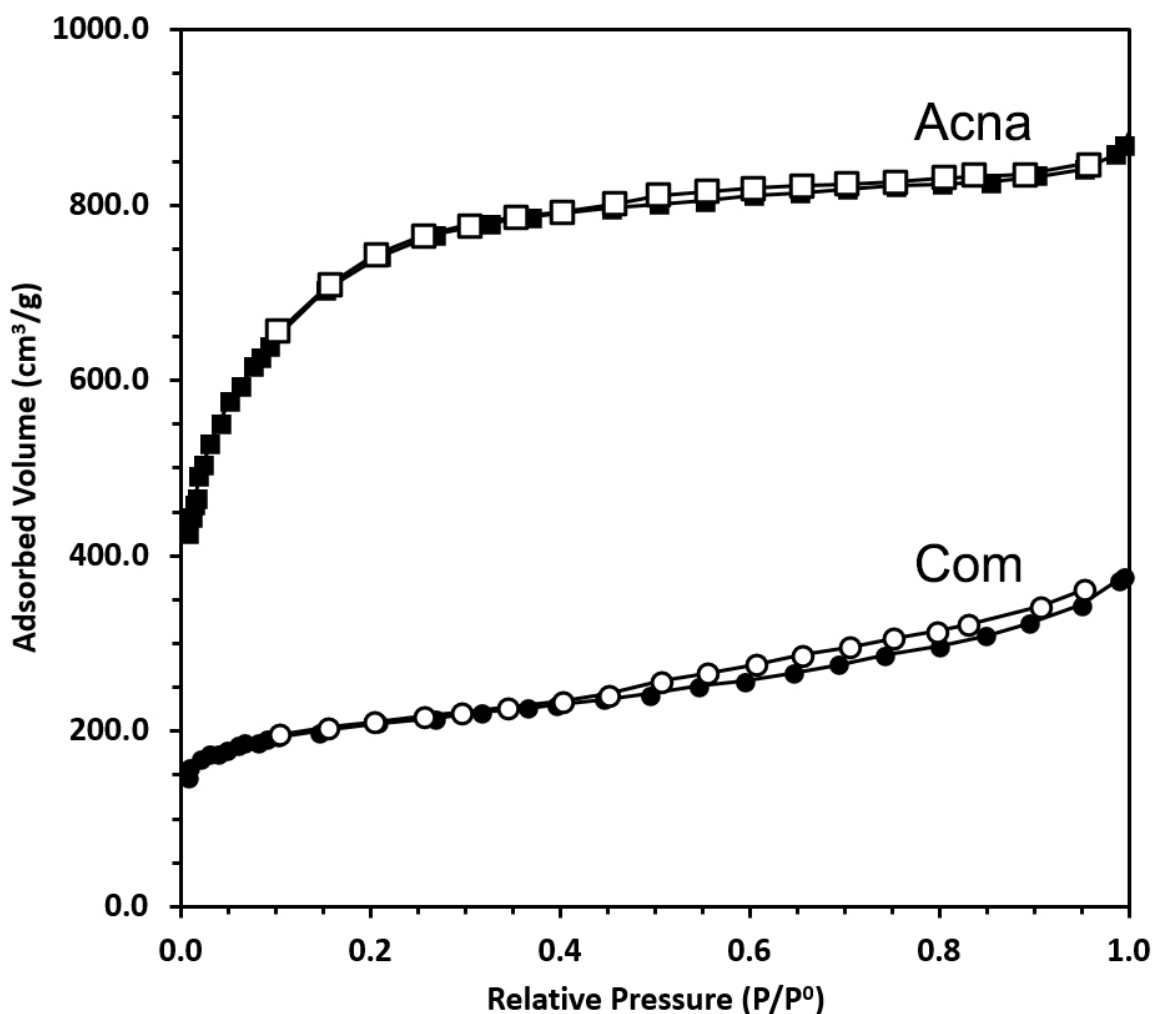
Figure 2. Adsorption and desorption isotherms of N2 at 77 K. for activated carbon samples.
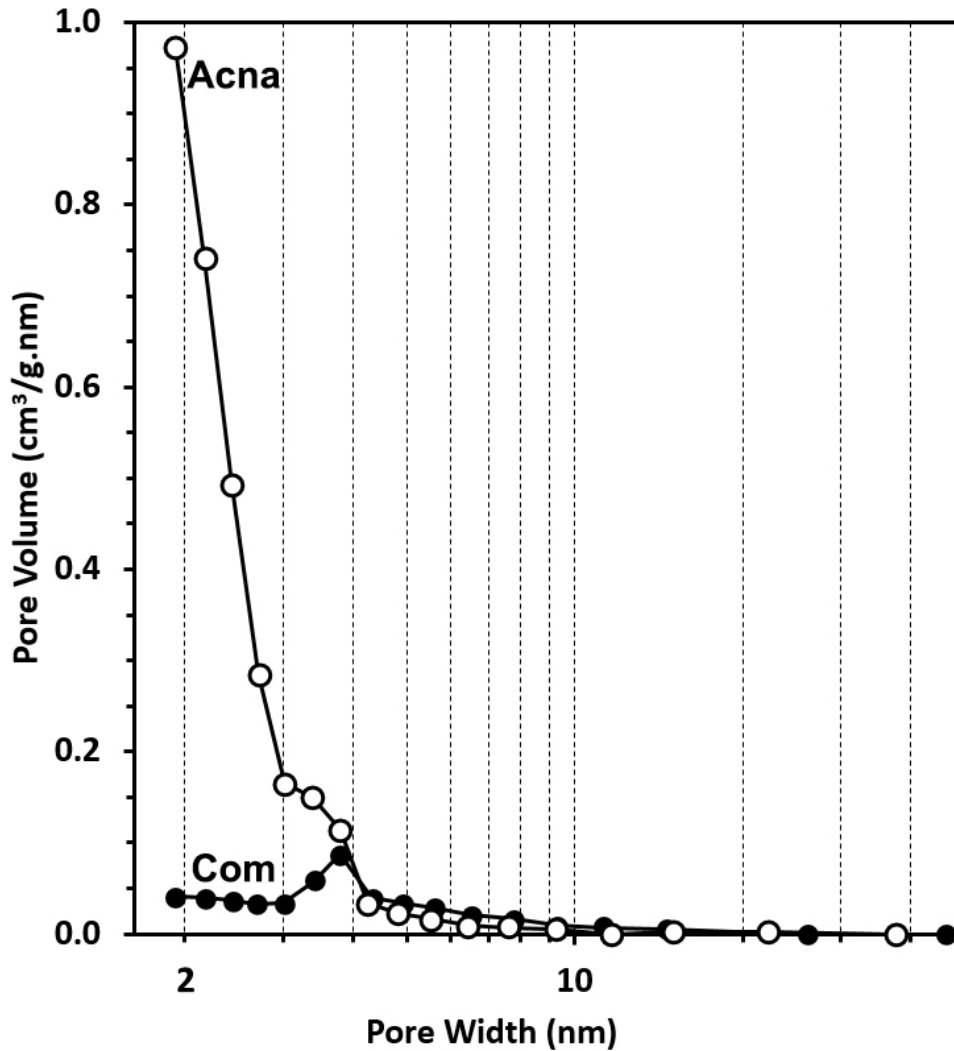
Figure 3. Pore size distribution of AC samples.

The pore size distribution of Com and Acna is presented in Figure 3. As discussed previously, the sunflower stalk based AC has mainly micropores. On the other hand, Com mainly consists of mesopores. Moreover, it should be mentioned that the sunflower stalk based activated carbon has a higher BET surface area than the commercial coal-based sample. The difference is more than 3 times of the Com sample. Although having a high specific surface area is very important, the nature of the pores also plays an important role in supercapacitor performance.

Electrochemical Characterization

For the electrochemical characterizations, two-electrode symmetrical cells were prepared. Figure 4 shows the cyclic voltammograms of supercapacitor cells of Com and Acna samples at different scan rates (1 - 200 mV) (10th cycle). The quasi-rectangular and symmetric shape of the current-voltage curves indicates a stable capacitive performance of the supercapacitor cells in the aqueous 1 M H_2SO_4 electrolyte. The steep charge and discharge curves show that the studied systems have a good electrochemical operation. The quasi-rectangular shape indicates that all the AC samples have a microporous structure in parallel to the textural characterization results. When the areas of the curves are compared, Acna samples has a bigger area and this suggests a higher capacitance. This area is big in lower scan rates as well and shows a good capacitive behavior [22-24]. It should be noted that CV curves, especially at high scan rates, reveal a spike at 0.8 V. Actually this spike is more pronounced in the Acna sample. This behavior discloses a fast charging and discharging non-Faradaic mechanism [25].
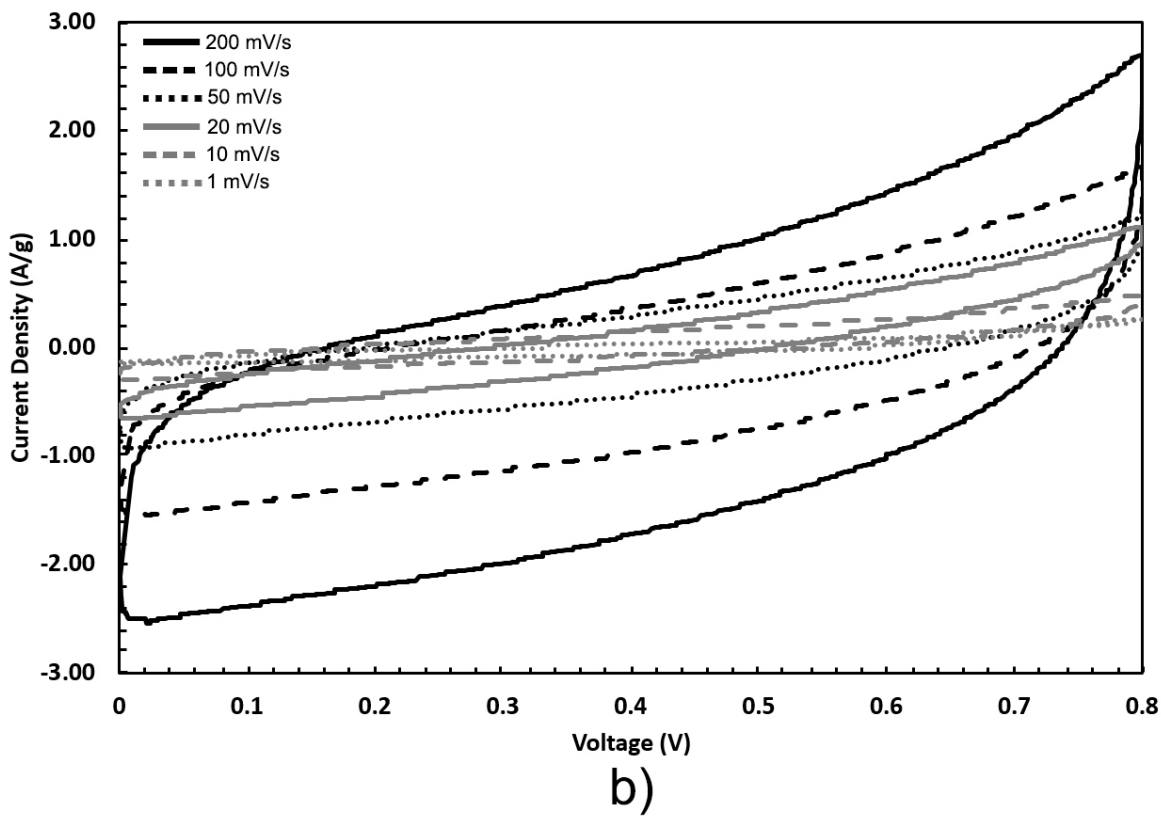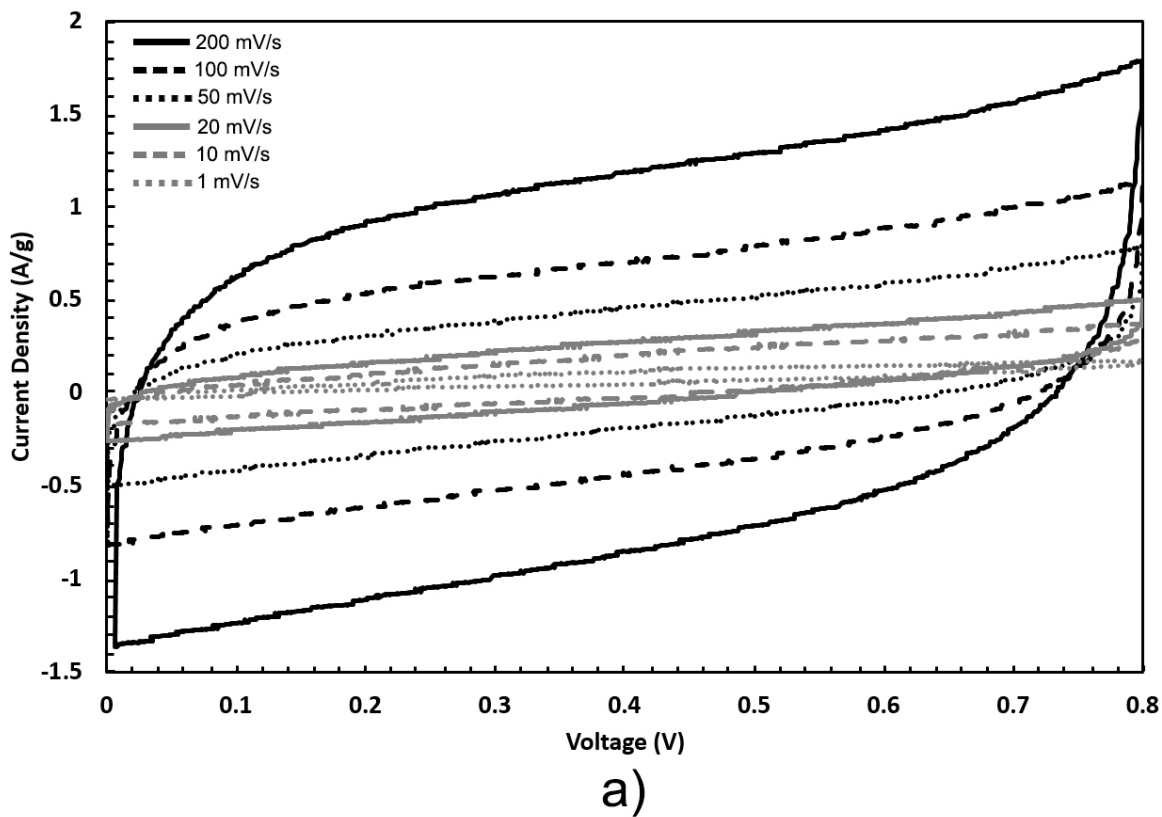
Figure 4. Cyclic voltammograms of a) Com and b) Acna cells at various scan rates.

Galvanostatic charge and discharge tests of the AC samples were performed under the current densities of 0.05-2 A/g between the voltage range of 0-0.8 V. For the two-electrode charge-discharge measurements, the specific gravimetric capacitance (SGC) is calculated using equation (1) [26]:

$$C_{SP} = \frac{4 I_{Cell} \Delta t}{m \Delta V_{Cell}} \qquad (1)$$

where ICell is the discharge current in amperes, Δt is the discharge time in seconds, ΔVCell is the cell potential window in volts, and m is the total mass of the active material on both electrodes in grams. Fig. 5 shows the charge-discharge curves of the two-electrode supercapacitor cells of Com and Acna at the tenth cycle for various current densities. The charge-discharge curves of Com show a symmetric triangle-like shape, which indicates a good capacitive behavior. However for Acna symmetric triangle-like shape can only be seen for high current densities (1 and 2 A/g), but at lower current densities a bend on the curve was observed. The reason for this bend is due to the high percentage of micropores. The specific capacitance of Com at 0.05 A/g is 93 F/g. On the other hand, at the same current density, Acna has a capacitance of 207 F/g. This result also coincides with the CV results. This big difference is probably due to the high specific surface area difference.
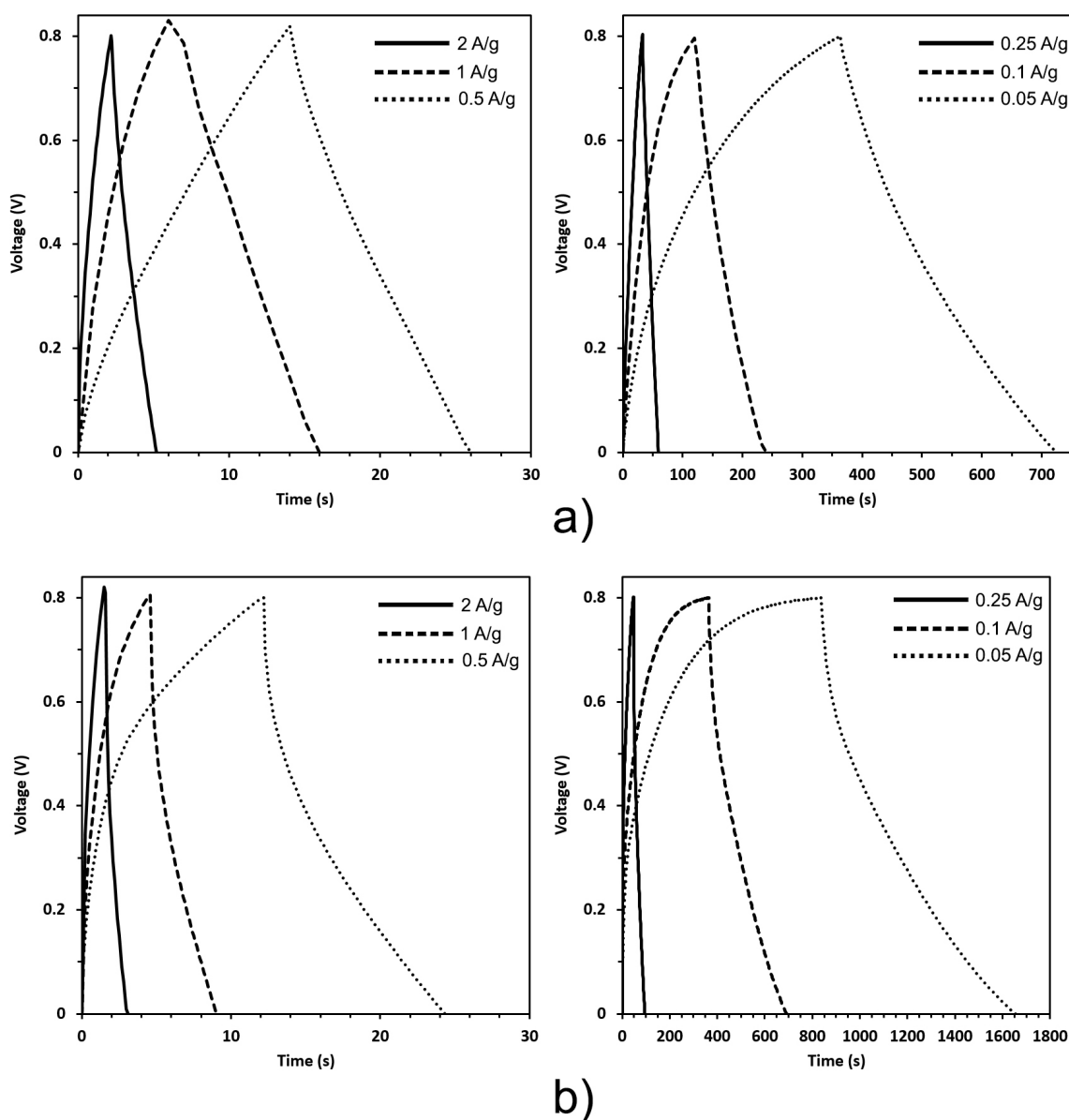
Figure 5. Galvanostatic charge-discharge curves of a) Com, and b) Acna.
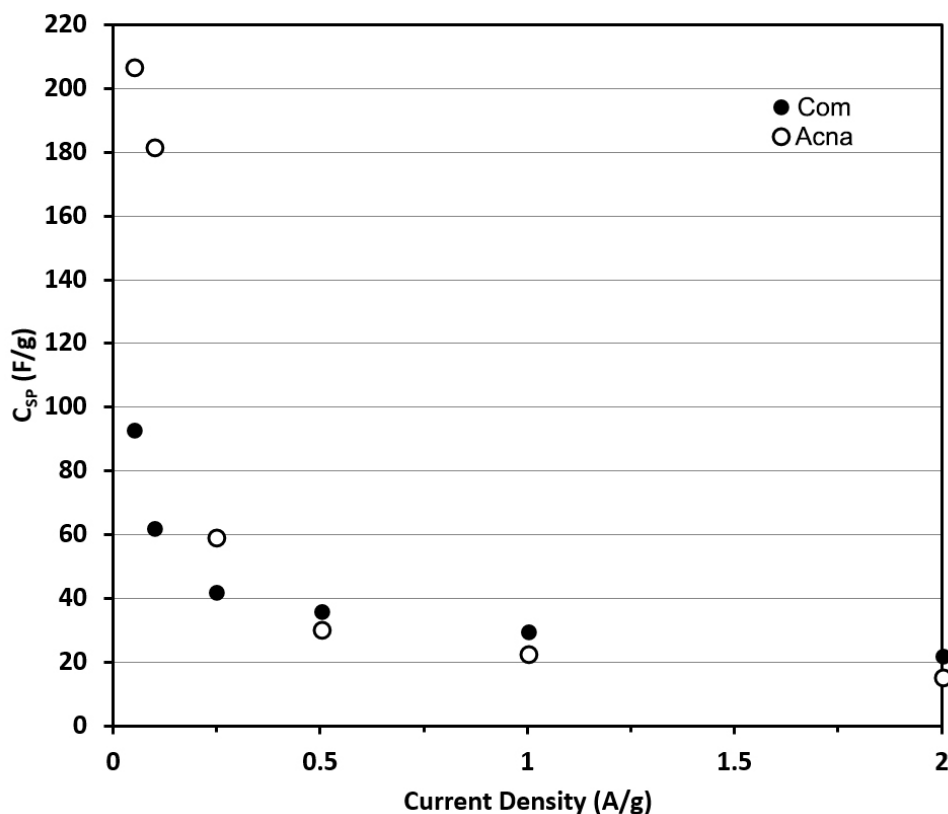
Figure 6. Variation of specific capacitance with different current densities.

Figure 6 shows the variation of specific capacitances with changing current densities. For both of the cases, as expected, with decreasing current densities, specific capacitance increases [24]. With higher current densities, less amount of ions accumulates at the AC/electrolyte interface. Interestingly from 0.5 to 2 A/g, Com exhibits higher capacitances. However starting from 0.5 A/g, Acna's capacitance increases with a very steep curve. This can be explained by the inability of micropores present in Acna to supply charges at high currents. The interaction between Acna micropores and the ions probably is not able to counterbalance this driving force. This results in the reduction of capacitance. But generally, the Acna cell shows better capacitances. Actually, with an increasing amount of micropores, the increase in capacitance at lower current densities becomes steeper [27]. The Acna sample showed similar behavior. In table 4, some biomass-based ACs and their properties are compared. As can be seen from this table, there is a huge difference in both specific surface areas and capacitances. Although all the capacitance values a very high, a high specific surface area does not necessarily mean a high capacitance. Every biomass has a different porous structure and reacts distinctly to the activation

agent. Of course, the pore size distribution and the interaction with the electrolyte also determine the performance. The hydrated ions should be small enough to penetrate deep into the micropores [28]. At high concentrations, the capacitance increases, but handling highly concentrated electrolytes can be hard and requires special containers, current collectors and separators. The effect of charge-discharge cycles on the cycle life of the supercapacitor cells was examined up to 10000 cycles at a current density of 1 A/g (Figure 7). The Com cell performs quite stable up to the 6500th cycle. However, after that point, the capacitance significantly drops and ends at about 70% of initial capacitance. On the other hand, Acna cell shows a 20% capacitance loss at the 1000th cycle but conserves this capacitance until the end of the 10000th cycle. It has been reported that ACs with higher micropore content perform better for longer charge-discharge cycles [25].

"The specific average energy (ESP) and power (PSP) densities were calculated using equations (2) and (3) according to capacitance values from galvanostatic discharge tests [34]:

$$E_{SP} = \frac{C_{SP}V_{Cell}^2}{7.2} \qquad (2)$$

$$P_{SP} = \frac{3600E_{SP}}{\Delta t} \qquad (3)$$

Table 4. . Comparison of some AC based supercapacitors.

AC Source	SBET (m²/g)	Activation Agent	Electrolyte	CSP (F/g)	Ref.
Apricot shell	2074	NaOH	6 M KOH	339	[29]
Birch sawdust	3300	NaOH	4.9 M H_2SO_4	310	[30]
Cherry stone	1273	KOH	2 M H_2SO_4	230	[31]
Sunflower stalk	2658	NaOH	1 M H_2SO_4	207	This Study
Rice husk	2681	NaOH	0.5 M K_2SO_4	172	[32]
Coconut kernel	1200	KOH	1 M H_2SO_4	173	[33]

Where ESP is in Wh/kg, PSP is in W/kg, CSP is in F/g and Δt is in s. Figure 8 shows the Ragone plot of the Com and Acna supercapacitor cells. Clearly, it can be seen that with increasing power density, energy density decreases. Usually, the energy and power densities depend on the porous structure and electrolyte/active material interaction. Due to the pore and electrolyte resistances, the power and energy density trend is inverse. Similar to the galvanostatic charge-discharge results, there are regions where each material performs better. Acna showed higher energy densities below 600 W/kg (18.4 Wh/kg at a power density of 80 W/kg) and Com showed higher energy densities above 600 W/kg. The large surface area of Acna enabled storing high amounts of charges however the high percentage of micropores did not let the release of these charges at high currents.
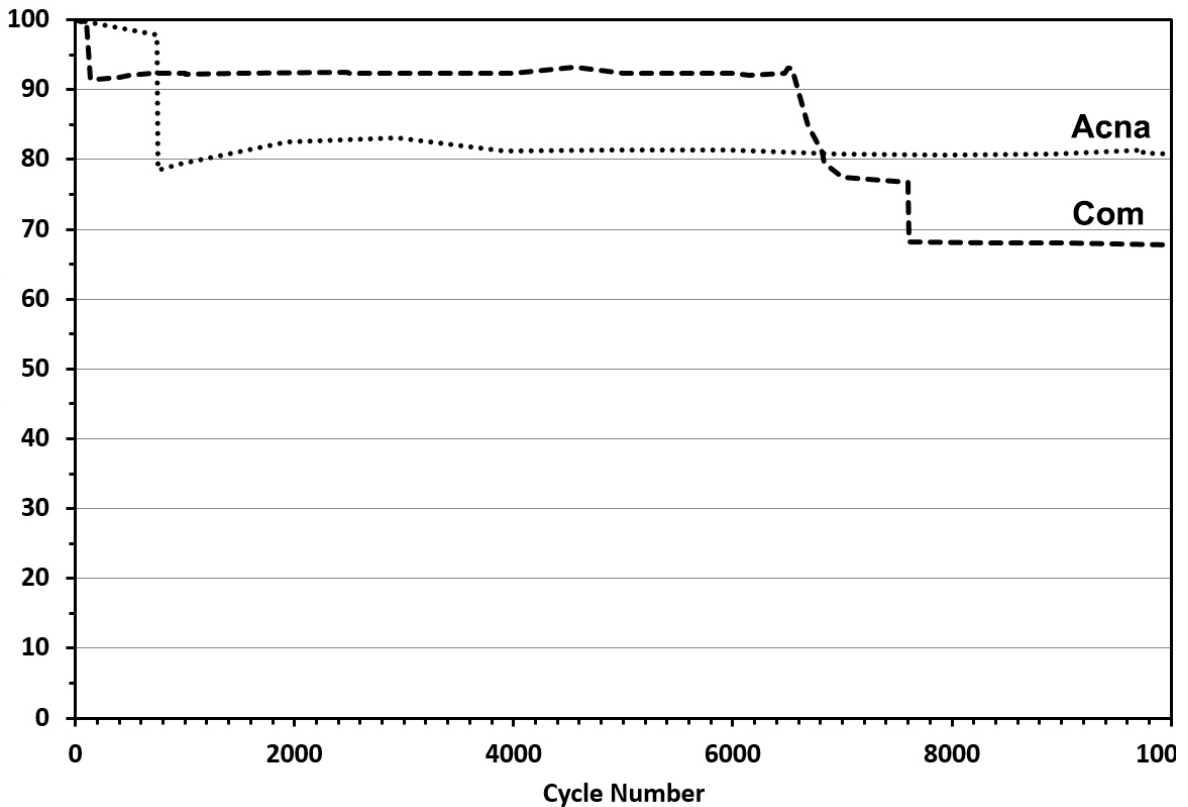
Figure 7. Effect of charge-discharge cycles on the lifetime of Com and Acna cells (1 A/g, 10000 cycles).
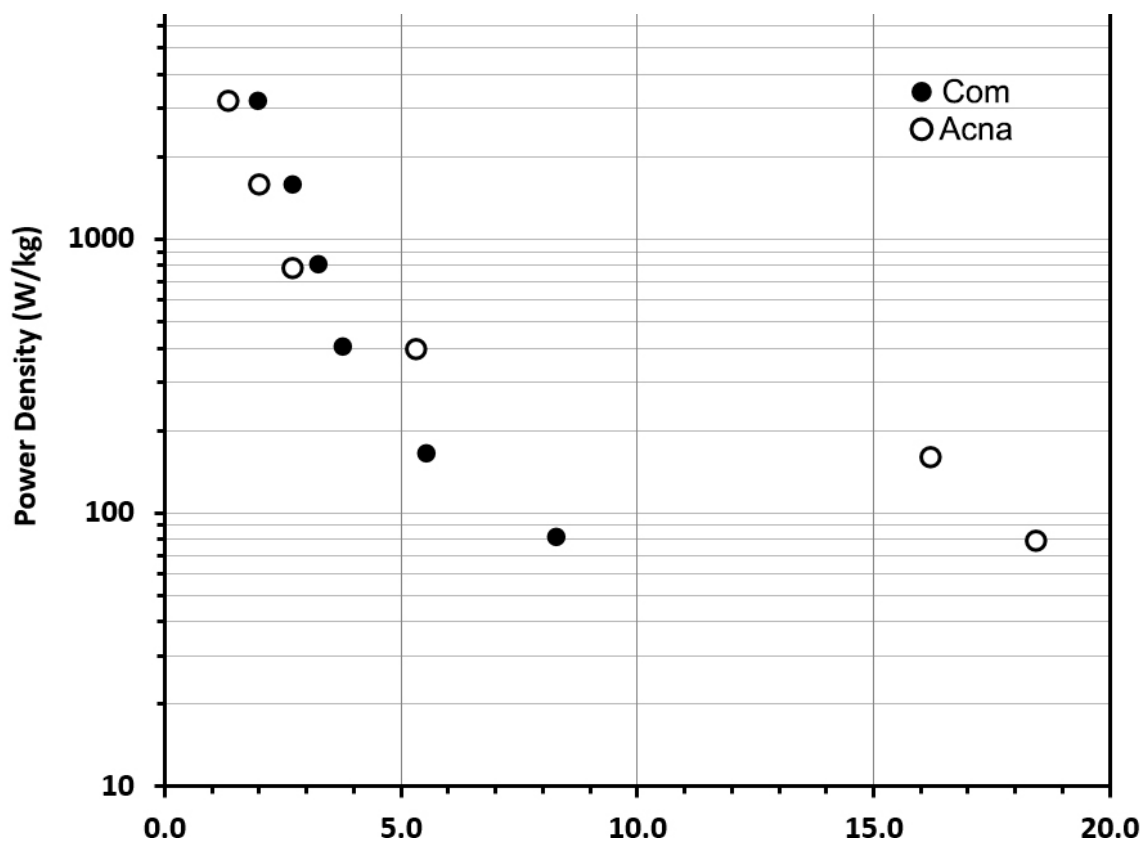
Figure 8. Ragone plots of Com and Acna supercapacitor cells.

Figure 9 shows the Nyquist plots of the Com and Acna cells, where small semi-circle (higher frequencies) and a straight line (lower frequencies) can be seen. While the semicircle suggests that there is an RC mechanism (a capacitor and a resistance connected in parallel) in the electrode, the nonvertical straight line is due to the diffusion resistance in the electrolyte. Generally, the electrochemical impedance of a supercapacitor fits a Randales Cell where series resistance (RESR) is in series with a parallel a constant phase element (non-ideal capacitor) and a Warburg element (diffusion resistance) with a charge transfer resistance (RCT). The obtained Nyquist plot fits this model perfectly. The high-frequency end of the semi-circle gives the equivalent series resistance (RESR) which is the combination of the contact resistance between the current collector and the electrode layer, the resistance of the electrolyte, etc.. For both of the cells RESR was about 0.4 Ω. The size of the semicircle is about the resistance inside the electrode [35]. According to Figure 9.b, Com cell has a lower electrode resistance than Acna cell. Moreover, the slope of Acna's straight line is smaller, this means that the diffusion resistance is higher for Acna [36, 37]. All this information

actually confirms the previous discussions about micropores resistance at high current densities.

CONCLUSIONS

As a summary, an activated carbon sample was prepared from sunflower stalk with a combination of chemical and physical activation. The sunflower-based AC (Acna) have a significantly high specific surface area with a high percentage of micropores. The obtained AC material was electrochemically characterized in a two-electrode supercapacitor cell. Acna showed a very high specific capacitance of 207 F/g at 0.05 A/g, an energy density of 18.4 Wh/kg at a power density of 80 W/kg. With a high specific surface area and a high percentage of micropores, very promising results were obtained. However, galvanostatic charge-discharge curves, cyclic voltammograms, and Nyquist plots reveal that Acna and H_2SO_4 electrolyte are not perfectly compatible. Aqueous electrolytes with neutral salts or nonaqueous electrolytes may even give better results.
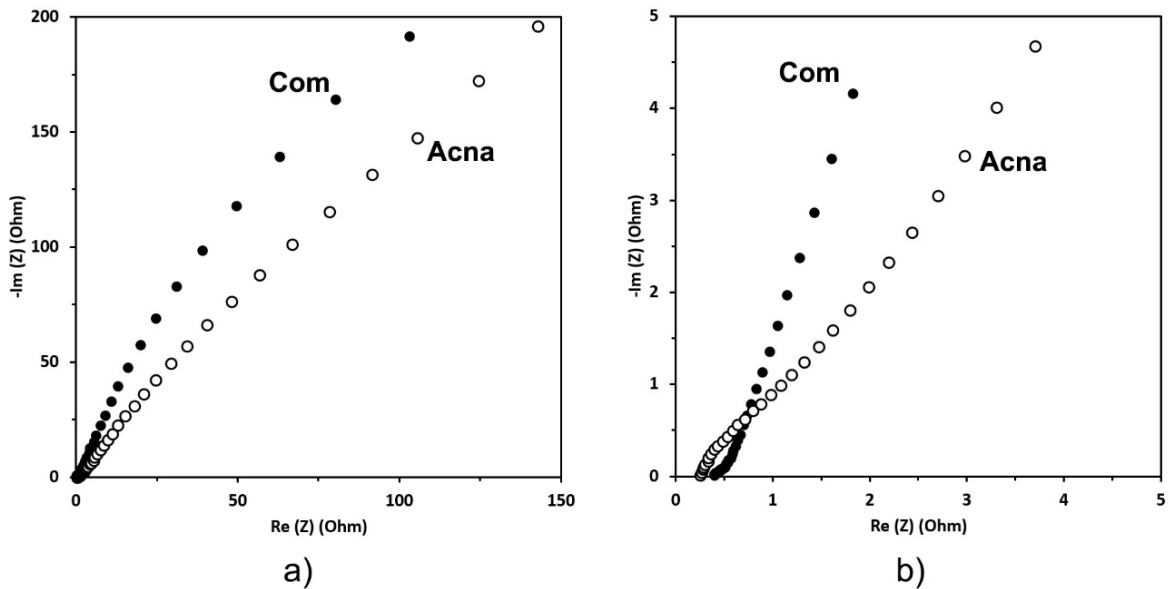
Figure 9. a) Nyquist plot of the Com and Acna samples after 10 cycles, and b) enlarged view of the Nyquist plot in the **high-frequency range.**

References

1. M.D.D. de Leon-Garza, E. Soto-Regalado, M. Loredo-Cancino, F.D. Cerino-Cordova, R.B. Garcia-Reyes, N.E. Davila-Guzman, J.A. Loredo-Medrano, Phenol adsorption onto coffee waste - granular activated carbon: kinetics and equilibrium studies in aqueous solutions, Desalin. Water Treat., 90 (2017) 231-240.

2. F.M. Kasperiski, E.C. Lima, C.S. Umpierres, G.S. dos Reis, P.S. Thue, D.R. Lima, S.L.P. Dias, C. Saucier, J.B. da Costa, Production of porous activated carbons from Caesalpinia ferrea seed pod wastes: Highly efficient removal of captopril from aqueous solutions, J. Clean Prod., 197 (2018) 919-929.

3. N.G. Rincon-Silva, J.C. Moreno-Pirajan, L. Giraldo, Removal of phenol, p-nitrophenol and p-chlorophenol from activated carbon chemically with sulfuric acid from lignocellulosic waste material: Effect of the concentration of activating agent, Afinidad, 74 (2017) 112-123.

4. W.Y. Ao, J. Fu, X. Mao, Q.H. Kang, C.M. Ran, Y. Liu, H.D. Zhang, Z.P. Gao, J. Li, G.Q. Liu, J.J. Dai, Microwave assisted preparation of activated carbon from biomass: A review, Renew. Sust. Energ. Rev., 92 (2018) 958-979.

5. M. Danish, T. Ahmad, A review on utilization of wood biomass as a sustainable precursor for activated carbon production and application, Renew. Sust. Energ. Rev., 87 (2018) 1-21.

6. P. Gonzalez-Garcia, Activated carbon from lignocellulosics precursors: A review of the synthesis methods, characterization techniques and applications, Renew. Sust. Energ. Rev., 82 (2018) 1393-1414.

7. Y.H. Cao, K.L. Wang, X.M. Wang, Z.R. Gu, Q.H. Fan, W. Gibbons, J.D. Hoefelmeyer, P.R. Kharel, M. Shrestha, Hierarchical porous activated carbon for supercapacitor derived from corn stalk core by potassium hydroxide activation, Electrochim Acta, 212 (2016) 839-847.

8. E.Y.L. Teo, L. Muniandy, E.P. Ng, F. Adam, A.R. Mohamed, R. Jose, K.F. Chong, High surface area activated carbon from rice husk as a high performance supercapacitor electrode, Electrochim Acta, 192 (2016) 110-119.

9. C.C. Hu, C.C. Wang, F.C. Wu, R.L. Tseng, Characterization of pistachio shell-derived carbons activated by a combination of KOH and CO_2 for electric double-layer capacitors, Electrochim Acta, 52 (2007) 2498-2505.

10. Y.J. Kim, B.J. Lee, H. Suezaki, T. Chino, Y. Abe, T. Yanagiura, K.C. Park, M. Endo, Preparation and characterization of bamboo-based activated carbons as electrode materials for electric double layer capacitors, Carbon, 44 (2006) 1592-1595.

11. Y.Y. Zhu, M.M. Chen, Y. Zhang, W.X. Zhao, C.Y. Wang, A biomass-derived nitrogen-doped porous carbon for high-energy supercapacitor, Carbon, 140 (2018) 404-412.

12. J. Pang, W.F. Zhang, H. Zhang, J.L. Zhang, H.M. Zhang, G.P. Cao, M.F. Han, Y.S. Yang, Sustainable nitrogen-containing hierarchical porous carbon spheres derived from sodium lignosulfonate for high-performance supercapacitors, Carbon, 132 (2018) 280-293.

13. M. Jalali, F. Aboulghazi, Sunflower stalk, an agricultural waste, as an adsorbent for the removal of lead and cadmium from aqueous solutions, J. Mater. Cycles. Waste., 15 (2013) 548-555.

14. E. Koseoglu, C. Akmil-Basar, Preparation, structural evaluation and adsorptive properties of activated carbon from agricultural waste biomass, Adv. Powder. Technol., 26 (2015) 811-818.

15. A.L. Cazetta, A.M.M. Vargas, E.M. Nogami, M.H. Kunita, M.R. Guilherme, A.C. Martins, T.L. Silva, J.C.G. Moraes, V.C. Almeida, NaOH-activated carbon of high surface area produced from coconut shell: Kinetics and equilibrium studies from the methylene blue adsorption, Chem. Eng. J., 174 (2011) 117-125.

16. V.K. Singh, E.A. Kumar, Thermodynamic analysis of single-stage and single-effect two-stage adsorption cooling cycles using indigenous coconut shell based activated carbon-CO_2 pair, Int. J. Refrig., 84 (2017) 238-252.

17. D. Ozcimen, A. Ersoy-Mericboyu, Characterization of biochar and bio-oil samples obtained from carbonization of various biomass materials, Renew. Energ., 35 (2010) 1319-1324.

18. K.Z. Qian, A. Kumar, K. Patil, D. Bellmer, D.H. Wang, W.Q. Yuan, R.L. Huhnke, Effects of biomass feedstocks and gasification conditions on the physiochemical properties of char, Energies, 6 (2013) 3972-3986.

19. R. Rajarao, I. Mansuri, R. Dhunna, R. Khanna, V. Sahajwalla, Study of structural evolution of chars during rapid pyrolysis of waste CDs at different temperatures, Fuel, 134 (2014) 17-25.

20. O. Uner, Y. Bayrak, The effect of carbonization temperature, carbonization time and impregnation ratio on the properties of activated carbon produced from Arundo donax, Micropor. Mesopor. Mat., 268 (2018) 225-234.

21. S.S. Brum, M.L. Bianchi, V.L. Silva, M. Goncalves, M.C. Guerreiro, L.C.A. de Oliveira, Preparation and characterization of activated carbon produced from coffee waste, Quim. Nova, 31 (2008) 1048-1052.

22. R.H. Liu, E.H. Liu, R. Ding, K. Liu, Y. Teng, Z.Y. Luo, Z.P. Li, T.T. Hu, T.T. Liu, Facile in-situ redox synthesis of hierarchical porous activated carbon@MnO_2 core/shell nanocomposite for supercapacitors, Ceram. Int., 41 (2015) 12734-12741.

23. S.X. Hu, S.L. Zhang, N. Pan, Y.L. Hsieh, High energy density supercapacitors from lignin derived submicron activated carbon fibers in aqueous electrolytes, J. Power Sources, 270 (2014) 106-112.

24. B.H. Lu, Z.A. Xiao, H. Zhu, W. Xiao, W.L. Wu, D.H. Wang, Enhanced capacitive properties of commercial activated carbon by re-activation in molten carbonates, J. Power Sources, 298 (2015) 74-82.

25. W. Cao, F. Yang, Supercapacitors from high fructose corn syrup-derived activated, Mater. Today Energy, 9 (2018) 406-415.

26. L.S. Ghadimi, N. Arsalani, A.G. Tabrizi, A. Mohammadi, I. Ahadzadeh, Novel nanocomposite of $MnFe_2O_4$ and nitrogen-doped carbon from polyaniline carbonization as electrode material for symmetric ultra-stable supercapacitor, Electrochim. Acta, 282 (2018) 116-127.

27. T.A. Centeno, F. Stoeckli, The role of textural characteristics and oxygen-containing surface groups in the supercapacitor performances of activated carbons, Electrochim Acta, 52 (2006) 560-566.

28. M. Inagaki, H. Konno, O. Tanaike, Carbon materials for electrochemical capacitors, J. Power. Sources, 195 (2010) 7880-7903.

29. B. Xu, Y.F. Chen, G. Wei, G.P. Cao, H. Zhang, Y.S. Yang, Activated carbon with high capacitance prepared by NaOH activation for supercapacitors, Mater. Chem. Phys., 124 (2010) 504-509.

30. A. Volperts, G. Dobele, A. Zhurinsh, D. Vervikishko, E. Shkolnikov, J. Ozolinsh, Wood-based activated carbons for supercapacitor electrodes with a sulfuric acid electrolyte, New Carbon Mater., 32 (2017) 319-326.

31. M. Olivares-Marin, J.A. Fernandez, M.J. Lazaro, C. Fernandez-Gonzalez, A. Macias-Garcia, V. Gomez-Serrano, F. Stoeckli, T.A. Centeno, Cherry stones as precursor of activated carbons for supercapacitors, Mater. Chem. Phys., 114 (2009) 323-327.

32. K.L. Van, T.T.L. Thi, Activated carbon derived from rice husk by NaOH activation and its application in supercapacitor, Prog. Nat. Sci-Mater., 24 (2014) 191-198.

33. B. Kishore, D. Shanmughasundaram, T.R. Penki, N. Munichandraiah, Coconut kernel-derived activated carbon as electrode material for electrical double-layer capacitors, J. Appl. Electrochem., 44 (2014) 903-916.

34. Y. Hu, T.S. Fisher, Suggested standards for reporting power and energy density in supercapacitor research, B. Mater. Sci., 41 (2018).

35. R. Farzana, R. Rajarao, B.R. Bhat, V. Sahajwalla, Performance of an activated carbon supercapacitor electrode synthesised from waste Compact Discs (CDs), J. Ind. Eng. Chem., 65 (2018) 387-396.

36. I.I.G. Inal, S.M. Holmes, A. Banford, Z. Aktas, The performance of supercapacitor electrodes developed from chemically activated carbon produced from waste tea, Appl. Surf. Sci., 357 (2015) 696-703.

37. J. Huang, Diffusion impedance of electroactive materials, electrolytic solutions and porous electrodes: Warburg impedance and beyond, Electrochim. Acta, 281 (2018) 170-188.